Photorealistic images of carpet cloaks

Jad C. Halimeh,[1,*] Tolga Ergin,[1] Jonathan Mueller,[1] Nicolas Stenger,[1] and Martin Wegener[1,2]

[1] *Institut für Angewandte Physik and DFG-Center for Functional Nanostructures (CFN), Karlsruhe Institute of Technology (KIT), D-76128 Karlsruhe, Germany*
[2] *Institut für Nanotechnologie, Karlsruhe Institute of Technology (KIT), D-76128 Karlsruhe, Germany*
**Jad.Halimeh@physik.uni-karlsruhe.de*

Abstract: Using home-built dedicated ray-tracing software, we simulate photorealistic images of sceneries in three dimensions including dielectric carpet cloaks – i.e., continuously varying refractive-index distributions that allow for invisibility cloaking of a bump in a metallic carpet. Results for the ideal and for a simplified cloak are shown. The presented material gives a visual and intuitive impression of the performance of different arrangements and might be ideally suited for communicating the concepts of transformation optics to the general public.

OCIS codes: (080.0080) Geometric optics; (230.3205) Invisibility cloaks; (160.3918) Metamaterials; (080.2710) Inhomogeneous optical media.

References and links

1. J. B. Pendry, D. Schurig, and D. R. Smith, "Controlling electromagnetic fields," Science **312**(5781), 1780–1782 (2006).
2. U. Leonhardt, "Optical conformal mapping," Science **312**(5781), 1777–1780 (2006).
3. U. Leonhardt, and T. G. Philbin, "General relativity in electrical engineering," N. J. Phys. **8**(10), 247 (2006).
4. U. Leonhardt, "Notes on conformal invisibility devices," N. J. Phys. **8**(7), 118 (2006).
5. D. Schurig, J. J. Mock, B. J. Justice, S. A. Cummer, J. B. Pendry, A. F. Starr, and D. R. Smith, "Metamaterial electromagnetic cloak at microwave frequencies," Science **314**(5801), 977–980 (2006).
6. W. Cai, U. K. Chettiar, A. V. Kildishev, and V. M. Shalaev, "Optical cloaking with metamaterials," Nat. Photonics **1**(4), 224–227 (2007).
7. V. M. Shalaev, "Physics. Transforming light," Science **322**(5900), 384–386 (2008).
8. J. Li, and J. B. Pendry, "Hiding under the carpet: a new strategy for cloaking," Phys. Rev. Lett. **101**(20), 203901 (2008).
9. U. Leonhardt, and T. Tyc, "Broadband invisibility by non-Euclidean cloaking," Science **323**(5910), 110–112 (2009).
10. R. Liu, C. Ji, J. J. Mock, J. Y. Chin, T. J. Cui, and D. R. Smith, "Broadband ground-plane cloak," Science **323**(5912), 366–369 (2009).
11. J. Valentine, J. Li, T. Zentgraf, G. Bartal, and X. Zhang, "An optical cloak made of dielectrics," Nat. Mater. **8**(7), 568–571 (2009).
12. L. H. Gabrielli, J. Cardenas, C. B. Poitras, and M. Lipson, "Silicon nanostructure cloaking at optical frequencies," Nat. Photonics **3**, 461–463 (2009).
13. J. H. Lee, J. Blair, V. A. Tamma, Q. Wu, S. J. Rhee, C. J. Summers, and W. Park, "Direct visualization of optical frequency invisibility cloak based on silicon nanorod array," Opt. Express **17**, 12928 (2009).
14. I. I. Smolyaninov, V. N. Smolyaninova, A. V. Kildishev, and V. M. Shalaev, "Anisotropic metamaterials emulated by tapered waveguides: application to optical cloaking," Phys. Rev. Lett. **102**(21), 213901 (2009).
15. N. A. Nicorovici, R. C. McPhedran, and G. W. Milton, "Optical and dielectric properties of partially resonant composites," Phys. Rev. B **49**(12), 8479–8482 (1994).
16. A. Alù, and N. Engheta, "Plasmonic materials in transparency and cloaking problems: mechanism, robustness, and physical insights," Opt. Express **15**(6), 3318–3332 (2007).
17. S. Andrew, Glassner, An Introduction to Ray Tracing (Morgan Kaufmann, 1989).
18. G. Dolling, M. Wegener, S. Linden, and C. Hormann, "Photorealistic images of objects in effective negative-index materials," Opt. Express **14**(5), 1842–1849 (2006).
19. N. A. P. Nicorovici, R. C. McPhedran, S. Enoch, and G. Tayeb, "Finite wavelength cloaking by plasmonic resonance," N. J. Phys. **10**(11), 115020 (2008).
20. E. Kallos, C. Argyropoulos, and Y. Hao, "Ground-plane quasicloaking for free space," Phys. Rev. A **79**(6), 063825 (2009).
21. http://www.aph.uni-karlsruhe.de/wegener/en/publications&year=2009

#118102 - $15.00 USD Received 2 Oct 2009; accepted 7 Oct 2009; published 12 Oct 2009

1. Introduction

Transformation optics [1–14] – including invisibility cloaking – has recently attracted considerable attention not only in the scientific community but also in the general public. By tailoring the *local* optical properties, optical space can be shaped in analogy to the *local* distortions of actual space-time due to massive bodies in general relativity. Wave optics [1,5–8], ray optics [2,9], and electrostatic simulations [15,16] for different arrangements have been discussed and early waveguide experiments [5,10–14] have been published. However, the most obvious visualization, namely the simulation of photorealistic images of sceneries including invisibility cloaking structures, has not been shown so far. While one might argue that such images contain no new information in principle, they can give a very intuitive and visual impression of the cloaking performance. Furthermore, such images are ideal for communicating the underlying scientific principles to the general public. In this letter, we present such photorealistic images for what we believe is the first time. We use the so-called carpet cloak as a simple example.

2. The Ray tracing

Ray tracing [17] is a well-known rendering technique that is based on geometrical optics. We have previously published photorealistic images of sceneries including homogeneous negative-refractive-index media [18] using the open-software ray-tracing simulation package "POV-Ray 3.6". We were originally tempted to believe that it would be rather easy and straightforward to incorporate continuously varying refractive-index profiles into this program package. This, however, is not at all the case. In essence, one needs about 10^7 discretization volumes to mimic the continuously varying refractive-index distribution of the carpet cloak (see below). "POV-Ray 3.6" is limited to rays not crossing more than a maximum of 256 interfaces. Thus, one of us (J.C.H.) has written a corresponding dedicated computer program. This program accounts for Snell's refraction at each external and internal interface. Furthermore, it accounts for reflections from ideal metal surfaces as well as for angle-dependent Fresnel reflections at the outer boundary of the dielectric cloaking structure. We assume unpolarized light and, thus, the effective intensity reflectance becomes the average of the intensity reflectance of s- and p-polarized light. Secondary reflections, i.e., rays that get reflected twice or more, are neglected. This is justified because we will see below that even the primary reflections are fairly weak. Reflections at internal interfaces inside the inhomogeneous cloaking structure are also neglected as they should not occur at all for a continuously varying refractive-index profile.

3. The carpet cloak

The first example that we consider is the *ideal* refractive-index distribution of the carpet cloak. The scenery is illustrated in Fig. 1. Here, an arbitrary object is hidden under a metallic carpet. To hide the presence of the resulting bump in the carpet, the carpet is covered by a structure with a tailored refractive-index profile shown in Fig. 2: If light is reflected from the top of this bump, it experiences a smaller optical pathlength compared to light reflected in absence of the bump. To compensate for that, the refractive index of the material just above the bump has to be larger than further away from the bump. Furthermore, the index just on the sides of the bump has to be lower than that of the surrounding. This compensates the additional optical pathlength that light rays impinging under oblique incidence onto the edge of the bump experience due to propagation through the introduced higher-index region on top of the bump.

#118102 - $15.00 USD Received 2 Oct 2009; accepted 7 Oct 2009; published 12 Oct 2009

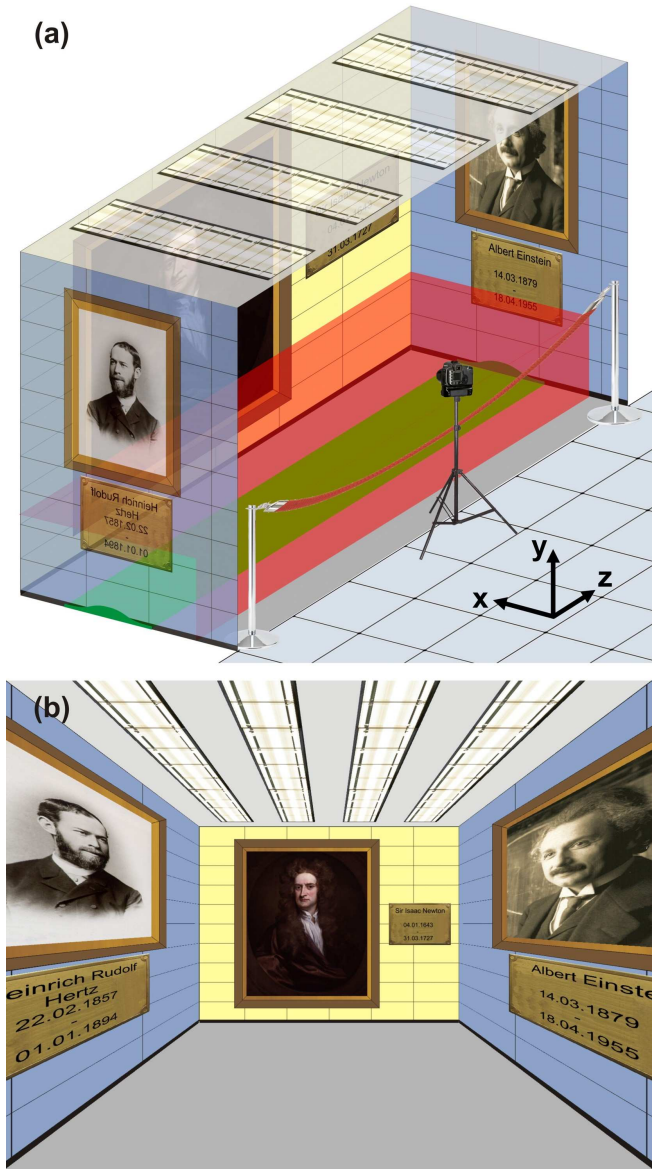

Fig. 1. (a) Artist's view of the scenery. A virtual camera with large field-of-view images a niche in a museum with portraits of famous scientists representing geometrical optics (Sir Isaac Newton), wave optics & electromagnetic waves (Heinrich Hertz), and quantum optics & general relativity (Albert Einstein), respectively. The bump on the floor (green) and the boundaries of the dielectric cloaking structure (red) are highlighted. (b) Resulting calculated image for a gray floor (i.e., no bump and no cloak).

This index distribution is scalable [8]. This scaling is done such that, far away from the bump, the refractive-index distribution approaches the so-called reference index. For our parameters, refractive indices below unity are avoided for a reference index of 1.20 (or higher). Thus, for an ideal carpet cloak with finite thickness, one eventually sees the metallic floor through a seemingly homogeneous transparent dielectric plate with the same finite thickness. One can neither see the hidden object nor the position of the bump. One does see, however, the influence of the dielectric plate, which is part of the carpet cloak structure and which leads to refraction and Fresnel reflections at its plane surface to the surrounding air.

#118102 - $15.00 USD Received 2 Oct 2009; accepted 7 Oct 2009; published 12 Oct 2009

Thus, even an ideal carpet cloak suffers from the "ostrich effect" [19], i.e., the cloak does make any object under the carpet invisible indeed, but the cloaking structure itself remains visible to some extent. (The ostrich is a large flightless bird native to Africa that sometimes sticks its head into the sand, leaving the rest of its body visible.) We will encounter the visual influence of the ostrich effect in our photorealistic images below.

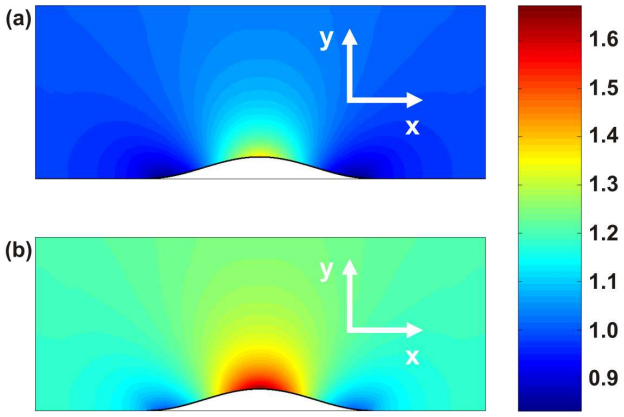

Fig. 2. False-color images of the refractive-index distribution of the cloaking structure (see also floor in Fig. 1(a)) in the *xy*-plane. The index is translationally invariant in the *z*-direction. (a) Reference index $n = 1.00$ (compare Fig. 3) and (b) $n = 1.20$ (compare Fig. 4). (a) and (b) are identical up to a factor of 1.20.

To allow for comparison with previous work, we choose a bump geometry similar to that in [10]. Precisely, our bump follows the form $y(x) = h \cos^2(\pi x/w)$ for $|x| \le w/2$ and zero otherwise. Here, h is the height of the bump and w is its full width. We choose $h/w = 9.6\%$. The extent of the entire cloaking structure is $2w$ in the x-direction and $10w/13$ in the y-direction. The refractive-index distribution in the entire cloaking structure is shown in Fig. 2. We have derived this index distribution numerically from the recipe given in [8]. Our two-dimensional index distribution is calculated on a mesh consisting of 104 times 40 points. As the three-dimensional ray-tracing calculations require a much higher spatial resolution (5200 times 2000), we have interpolated the coarse map. This interpolation is actually shown in Fig. 2. We have checked by calculations (not shown) using the *Comsol Multiphysics* software package similar to the ones published in [8] that our index profile delivers wave-optics cloaking results closely similar to those in [8]. Dispersion, i.e., a frequency dependence of the locally varying refractive index, n, is completely neglected, allowing for color images. This approximation is quite reasonable for the present circumstances because dielectrics with more or less constant indices in the range of $n = 1$ to $n = 2$ are readily available at around visible frequencies. If dispersion would be significant, the sceneries rendered below should simply be viewed as monochromatic images.

The cloaking structure is discretized by 5200 times 2000 cells in the *xy*-plane that have the width of the room in the *z*-direction (see Fig. 1(a)). This accounts for the translational invariance of the refractive-index distribution along z. We have carefully checked that this number of cells is sufficient for obtaining convergent ray-tracing results for a given refractive-index distribution. To be able to compare with analytically exact results, we have chosen a test refractive-index distribution following the form $n(y) = H/y$ for $0 \le y \le H$ and $n = 1$ otherwise, where $y = 0$ is the bottom and $y = H$ is the top of the structure. Based on Fermat's principle, we find that a ray impinging under oblique incidence experiences a displacement along the x-direction at height $y = H$ equal to

$$\Delta x = 2H \frac{1-\cos\alpha}{\sin\alpha}. \qquad (1)$$

#118102 - $15.00 USD Received 2 Oct 2009; accepted 7 Oct 2009; published 12 Oct 2009

Here, α is the angle of incidence with respect to the surface normal. The numerically computed and the exact analytically calculated displacement are compared for a bundle of 470 rays in the *xy*-plane with angles of incidence relative to the surface normal between 31° and 70°. We find that the mean relative error asymptotically scales with the number of layers N according to $\propto 1/N$. For example, for $N = 2000$, the mean relative error becomes 3.44×10^{-4} (with a standard deviation with respect to the bundle of rays of 1.8×10^{-4}).

For the rendered ray-tracing images, we need to define the field of view (FOV) of the virtual camera. The human *total* vertical (lateral) FOV in one eye is about 130° (169°), but this includes peripheral and ambient areas in the eye image where the eye does not focus. Problems with imperfect cloaking at large angles might be hidden in the human *focal* FOV. The virtual camera illustrated in Fig. 1(a) has a vertical (lateral) FOV of about 118° (131°). We have chosen this FOV, essentially corresponding to a wide-angle lens on the camera, to grasp a large fraction of the entire solid angle. A first example is shown in Fig. 1(b). Here, for reference, the floor is gray and non-reflecting. Clearly, the large FOV leads to an image that differs from what the human eye would perceive. This effect will be present in all following images.

Figures 3 and 4 show rendered photorealistic images corresponding to the scenery of Fig. 1. The corresponding reference indices are 1.00 (compare Fig. 2(a)) and 1.20 (compare Fig. 2(b)), respectively. In Fig. 3(a), the floor is metallic, leading to obvious reflections. In Fig. 3(b), the bump is introduced. While the bump is actually quite shallow (compare Fig. 1), its influence on the virtual image is obviously drastic: one can clearly see a reflection of the ceiling lamps. Furthermore, Newton's reflection from the floor is barely recognizable and Hertz' right cheek as well as Einstein's left cheek are double-reflected from the bump. The cloaking structure is added in Fig. 3(c). This largely recovers the original view in (a). Yet, certain distortions do remain even for a view straight ahead onto Newton's face, which appears slightly shifted. This aspect is likely partly due to the approximation of a locally isotropic refractive index underlying the carpet cloak design. An ideal cloak would require an anisotropic index distribution and even a magnetic permeability different from unity. In fact, small distortions of the carpet cloak are also visible in previously published wave-optics calculations [8]. However, we cannot completely exclude an effect of the finite precision in our numerical calculations of the refractive-index profile. In contrast, we have carefully checked that the ray-tracing is fully converged (see discussion above). The images rendered by ray-tracing simply turn out to be extremely sensitive to even minute details of the refractive-index profile.

By its two-dimensional design, the ideal two-dimensional carpet cloak [8] should only be perfect for a view straight ahead onto Newton's face. The virtual camera, however, also "sees" rays coming from the left-hand side and the right-hand side of the scenery. Hence, as expected, the corresponding image distortions in Fig. 3(c) are much larger than for a view straight ahead onto Newton's face. For example, the (originally straight) edges of Newton's name plate are strongly curved in their reflections on the floor. Intuitively, part of these distortions originate from the fact that rays impinging under an angle effectively experience a wider bump, hence a different height-to-width ratio of the bump, leading to an effectively incorrect refractive-index profile. Nevertheless, the carpet cloak is still performing amazingly well even under these wide-angle conditions.

The images in Fig. 4 for a reference index of 1.20 show the expected changes/shifts. The shifts due to the dielectric plate on the floor (also see Fig. 1) can be seen by comparing Fig. 3(a) and Fig. 4(a). An absolutely perfect carpet cloak with refractive indices larger than unity is expected to look like Fig. 4(a). The dielectric plate leads to additional reflections (see, e.g., the reflections from Hertz' and Einstein's name plate) and to an apparent bending of the bottom of the rear wall due to refraction at its interface to air – two aspects of the ostrich effect addressed above.

#118102 - $15.00 USD Received 2 Oct 2009; accepted 7 Oct 2009; published 12 Oct 2009

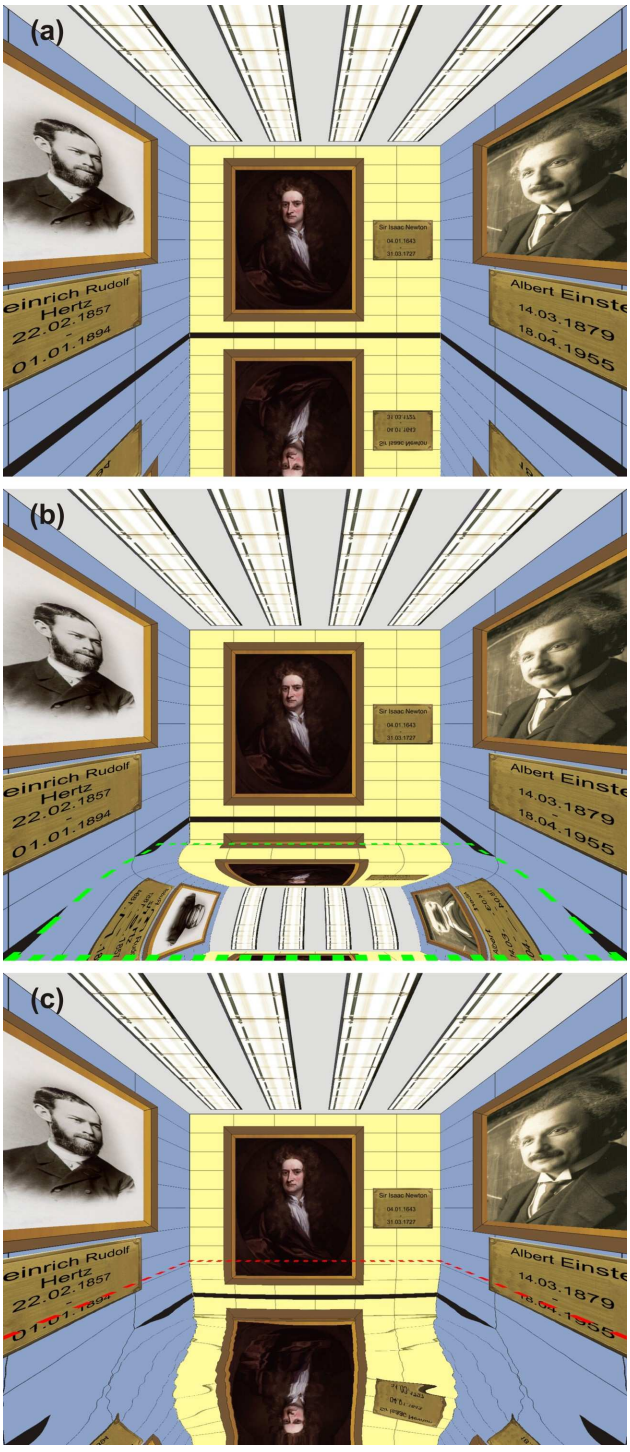

Fig. 3. Rendered images seen by the virtual camera of Fig. 1(a). (a) Metallic (hence reflecting) floor, (b) as (a) but with a bump whose edges are outlined in green (see also green outline within cloak in Fig. 1), (c) as (b) but with the cloaking structure added (top outlined in red). The index distribution corresponds to that shown in Fig. 2(a), i.e., the reference index is unity.

#118102 - $15.00 USD Received 2 Oct 2009; accepted 7 Oct 2009; published 12 Oct 2009

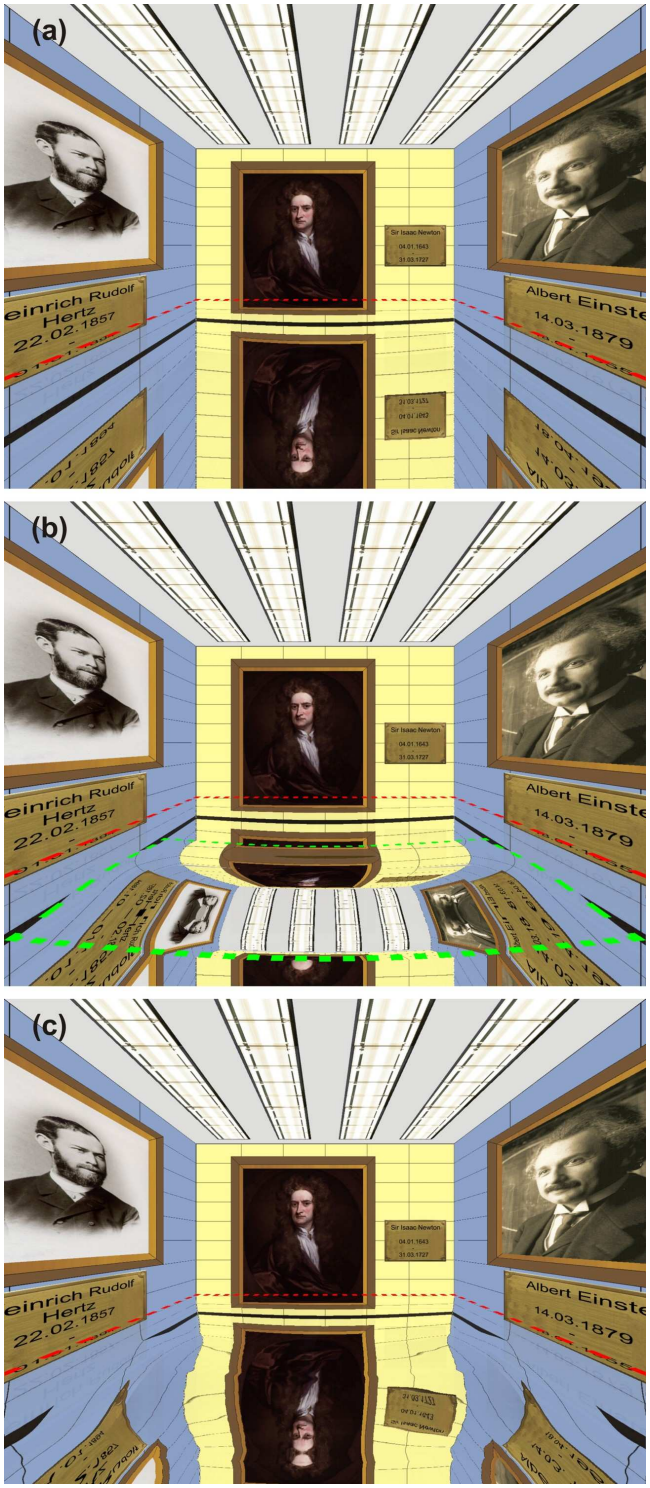

Fig. 4. As Fig. 3 but for a cloaking structure with a reference index equal to 1.20. Unlike in Fig. 3, both (a) and (b) include a dielectric plate with the reference index of 1.20 and with the same height as the cloak. In (a)-(b) and (c), the tops of the dielectric medium and the cloak, respectively, are outlined in red.

#118102 - $15.00 USD Received 2 Oct 2009; accepted 7 Oct 2009; published 12 Oct 2009

Some of our above findings have suggested that the visual impression in ray optics is much more sensitive to small refractive-index changes than in wave-optics calculations. To further investigate and emphasize this aspect, Fig. 5(b) shows the rendered image for a simplified refractive-index distribution defined in Fig. 5(a). Similar drastically simplified profiles with only a few "blocks", each with a constant refractive index within, have previously led to rather good cloaking performance in wave-optics calculations [20]. Again, we have obtained comparable results in our own *Comsol Multiphysics* wave-optics calculations (not shown). In contrast, the deviations from an ideal cloak are gigantic in our ray-optics calculations – an aspect that can be seen by comparing Fig. 4(c) and Fig. 5(b). Recall that we have again neglected internal reflections inside the carpet cloak. This approximation is not very well justified for Fig. 5(b), however, incorporating the additional partial reflections from these internal interfaces is expected to further deteriorate the images in Fig. 5(b) – which would further increase the differences between Fig. 4(c) and Fig. 5(b).

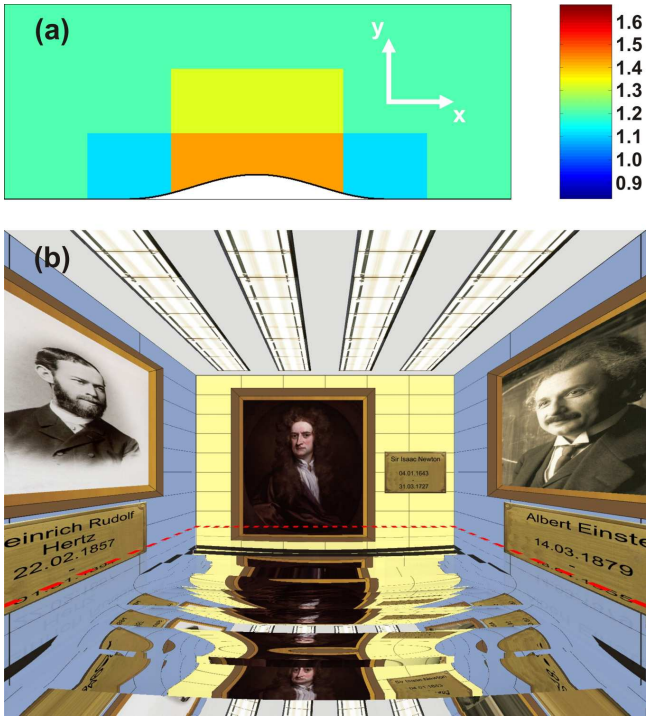

Fig. 5. (a) Simplified refractive index distribution roughly mimicking that of Fig. 2(b). The reference index is 1.20. (b) Corresponding rendered image.

This very large difference between wave optics and ray optics might be surprising at first sight. However, one must simply recall that ray optics is the limit of zero wavelength of light. Hence, the light field "sees" each and every detail. In contrast, in wave optics, the wave tends to average over structures smaller than the wavelength scale. Indeed, in the mentioned wave-optics calculations [20], the wavelength has been comparable to or even larger than the size of the blocks. Hence, the light wave has not "seen" these details. Wave-optics calculations for sceneries with sizes many orders of magnitude larger than the wavelength of light are currently way out of reach in terms of computational feasibility. Therefore, a ray-optics-based approach is presently best suited for visualizing macroscopic sceneries including inhomogeneous media.

4. Conclusions

Using a dedicated home-built ray-tracing program, we have rendered photorealistic images of sceneries including carpet cloaks. These images simply aim at giving an intuitive and visual

#118102 - $15.00 USD Received 2 Oct 2009; accepted 7 Oct 2009; published 12 Oct 2009

understanding of the concepts of transformation optics not only to scientists but also to laymen (high-resolution images can be downloaded [21]). Moreover, we find that such geometrical-optics images tend to be much more susceptible to small index changes within the tailored structure than wave-optics calculations.

Acknowledgements

We thank Kurt Busch (and members of his group) for critical comments regarding the numerical implementation, for stimulating discussions, and for a reading of this manuscript. We thank J. Fischer for discussions regarding the numerical calculations of the refractive-index profiles. We acknowledge support by the Deutsche Forschungsgemeinschaft (DFG) and the State of Baden-Württemberg through the DFG-Center for Functional Nanostructures (CFN) within subproject A1.5. The project PHOME acknowledges the financial support of the Future and Emerging Technologies (FET) programme within the Seventh Framework Programme for Research of the European Commission, under FET-Open grant number 213390. The project METAMAT is supported by the Bundesministerium für Bildung und Forschung (BMBF). J.C.H. and N.S. are supported by the Karlsruhe School of Optics & Photonics (KSOP). The PhD education of T.E. is embedded in KSOP.

#118102 - $15.00 USD Received 2 Oct 2009; accepted 7 Oct 2009; published 12 Oct 2009